Neurotherapeutics (2023) 20:1154–1166
https://doi.org/10.1007/s13311-023-01382-4

ORIGINAL ARTICLE

Inhibition of ACSL4 Alleviates Parkinsonism Phenotypes by Reduction of Lipid Reactive Oxygen Species

Fei Tang[1] · Liu-yao Zhou[1] · Ping Li[1] · Ling-ling Jiao[1] · Kang Chen[1] · Yu-jie Guo[1] · Xu-long Ding[1] · Si-yu He[1] · Biao Dong[1] · Ru-xiang Xu[2,3] · Huan Xiong[1,2,3] · Peng Lei[1]

Accepted: 9 April 2023 / Published online: 3 May 2023

Abstract

Ferroptosis is a programmed cell death pathway that is recently linked to Parkinson's disease (PD), where the key genes and molecules involved are still yet to be defined. Acyl-CoA synthetase long-chain family member 4 (ACSL4) esterifies polyunsaturated fatty acids (PUFAs) which is essential to trigger ferroptosis, and is suggested as a key gene in the pathogenesis of several neurological diseases including ischemic stroke and multiple sclerosis. Here, we report that ACSL4 expression in the substantia nigra (SN) was increased in a 1-methyl-4-phenyl-1,2,3,6-tetrahydropyridine (MPTP)-treated model of PD and in dopaminergic neurons in PD patients. Knockdown of ACSL4 in the SN protected against dopaminergic neuronal death and motor deficits in the MPTP mice, while inhibition of ACSL4 activity with Triacsin C similarly ameliorated the parkinsonism phenotypes. Similar effects of ACSL4 reduction were observed in cells treated with 1-methyl-4-phenylpyridinium (MPP^+) and it specifically prevented the lipid ROS elevation without affecting the mitochondrial ROS changes. These data support ACSL4 as a therapeutic target associated with lipid peroxidation in PD.

Keywords ACSL4 · Parkinson's disease · Neuroprotection · Ferroptosis · Lipid peroxidation

Introduction

Parkinson's disease (PD) is characterized by motor dysfunction and nonmotor symptoms, and it affects more than 6 million individuals worldwide [1]. One key pathology of PD is the progressive and irreversible loss of dopaminergic neurons in the substantia nigra (SN), which can be therapeutically targeted. However, current therapies for PD, such as levodopa medication or deep brain stimulation, are only symptomatic and cannot prevent neurodegeneration [2]. A variety of programmed cell death pathways may be responsible for dopaminergic neuronal loss in PD [3, 4], without the discovery of clinically successful drugs to date.

Ferroptosis is characterized by disrupted iron and glutathione metabolism, with the build-up of reactive oxygen species (ROS) within cells [5–7]; all of these features are also present in patients with PD as well as PD models [3, 8]. Indeed, the chelation of iron to rescue parkinsonism phenotypes has been tested in multiple animal models [9–13] and is currently undergoing phase III clinical trials for PD [13–15]. Subsequently, the general effect of ferroptosis in PD has been tested, by applying ferroptosis inhibitor ferrostatin-1 (Fer-1) or deferoxamine (DFO) to cells and animal models of PD [16–19]. However, these ferroptosis inhibitors are not blood–brain-barrier permeable, and therefore it is still in need to identify the key molecules that are responsible for ferroptosis execution during PD pathogenesis for future drug development.

Acyl-CoA synthase long-chain family member 4 (ACSL4) is a critical enzyme to catalyze the esterification of arachidonic acid (AA) and adrenaline into phytosterol

Fei Tang and Liu-yao Zhou contributed equally to this work.

✉ Huan Xiong
huan_xiong@163.com

✉ Peng Lei
peng.lei@scu.edu.cn

[1] State Key Laboratory of Biotherapy and National Clinical Research Center for Geriatrics, West China Hospital, Sichuan University, Sichuan 610041, China

[2] Department of Neurosurgery, Sichuan Provincial People's Hospital, University of Electronic Science and Technology of China, Chengdu 610072, China

[3] Chinese Academy of Sciences Sichuan Translational Medicine Research Hospital, Chengdu 610072, China

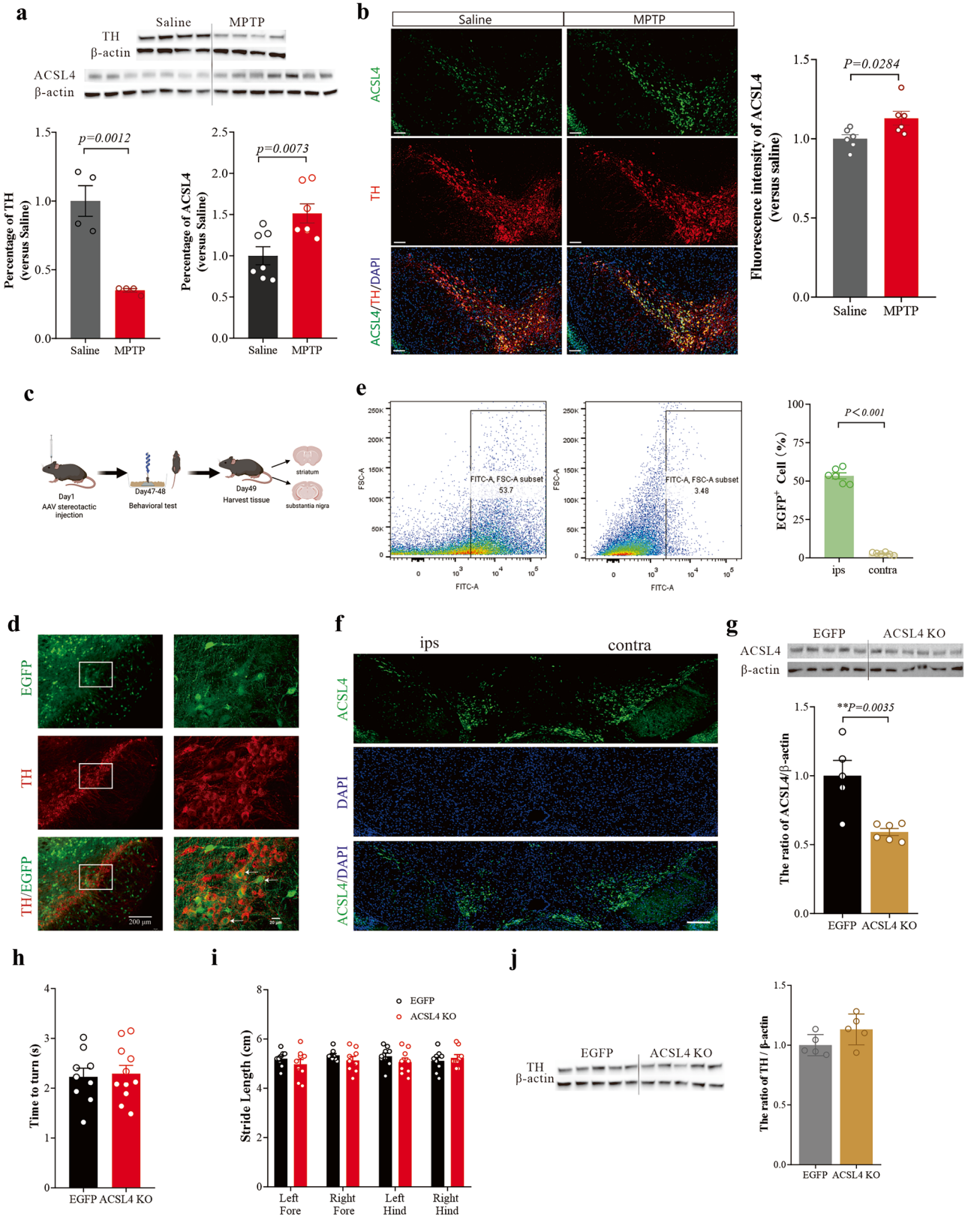
a
Saline
MPTP
TH
β-actin
ACSL4
β-actin
p=0.0012
Percentage of TH (versus Saline)
Saline
MPTP
p=0.0073
Percentage of ACSL4 (versus Saline)
Saline
MPTP
b
Saline
MPTP
ACSL4
TH
ACSL4/TH/DAPI
P=0.0284
Fluorescence intensity of ACSL4 (versus saline)
Saline
MPTP
c
Day1
AAV stereotactic injection
Day47-48
Behavioral test
Day49
Harvest tissue
striatum
substantia nigra
e
FITC-A, FSC-A subset
53.7
FITC-A, FSC-A subset
3.48
FSC-A
FITC-A
P<0.001
EGFP+ Cell (%)
ips
contra
d
EGFP
TH
TH/EGFP
200 μm
f
ips
contra
ACSL4
DAPI
ACSL4/DAPI
g
EGFP
ACSL4 KO
ACSL4
β-actin
**P=0.0035
The ratio of ACSL4/β-actin
EGFP
ACSL4 KO
h
Time to turn (s)
EGFP
ACSL4 KO
i
EGFP
ACSL4 KO
Stride Length (cm)
Left Fore
Right Fore
Left Hind
Right Hind
j
EGFP
ACSL4 KO
TH
β-actin
The ratio of TH / β-actin
EGFP
ACSL4 KO

◂**Fig. 1** Elevated ACSL4 expression levels in the SN in PD and the effects of SN ACSL4 KO in the brain. **a** TH and ACSL4 expressions in the SNs of MPTP-injected mice were determined by western blot analysis. **b** Representative images and the quantifications of ACSL4 and TH immunofluorescence staining in saline- or MPTP-treated mice. Scale bar = 200 μm. **c** Experimental scheme of AAV injection and the time point of phenotype detection. **d** Immunofluorescence staining has shown EGFP-positive cells and TH-positive neurons in the SN. The arrows indicate the co-labeled neurons. The scale bars represent 200 μm (left) and 20 μm (right). **e** Representative images (left, middle) and quantification (right) of EGFP-positive neurons in the ipsilateral and contralateral SN post-AAV-EGFP vector injection as detected with flow cytometry. **f** The expression of ACSL4 in the ipsilateral and contralateral SN post-AAV-ACSL4-KO vector injection. Scale bar = 200 μm. **g** ACSL4 was downregulated in the SN post-AAV-ACSL4-KO vector injection. **h** In the pole test, the time to turn was similar between the ACSL4-KO group and the EGFP group. **i** The gait parameters, stride length, were no different between the EGFP and ACSL4-KO groups. **j** The expression of TH was unaltered between the ACSL4-KO group and the EGFP group. The data are the means ± SEMs, and each point in the histogram represents a sample. *t*-Tests were performed. The *p* value is labeled in the histogram or is not displayed if it was higher than 0.05

esters, a process key to ROS accumulation during ferroptosis [20]. Inhibition of ACSL4 has been shown to prevent ferroptosis in animal models of several neurological diseases such as ischemic stroke, subarachnoid hemorrhage, and multiple sclerosis [21–23], and other diseases such as intestinal ischemia, diabetic retinopathy, and nonalcoholic fatty liver disease [24–26]. Interestingly, a retrospective cohort study has shown that the incidence of PD was reduced in patients with diabetes using glitazone antidiabetic drugs such as rosiglitazone and pioglitazone [27], and pioglitazone was neuroprotective against MPTP in mice [28]. Glitazones were found to be selective inhibitors of ACSL4, in addition to their roles as ligands of peroxisome proliferator-activated receptor γ (PPARγ) [29]. Thus, we hypothesized that ACSL4 participates in PD and that inhibition of ACSL4 ameliorates parkinsonism phenotypes.

To investigate the potential role of ACSL4 in PD, we reanalyzed the human SN expression data generated previously and validated the ACSL4 level in the PD animal model. We then genetically or pharmacologically targeted ACSL4 in the SN to test its impact on the parkinsonism phenotypes. We also explored the potential mechanism for ACSL4 action. These results may indicate ACSL4 as a therapeutic target to prevent neuronal death in PD.

Results

ACSL4 Is Upregulated in the MPTP Mice Model of Parkinsonism

The SN is the pivotal area for PD-related dopaminergic neurodegeneration. We first examined the ACSL4 protein level in SN, and found it was significantly elevated in the MPTP mouse model of PD compared to normal mice (Fig. 1a). The expression of tyrosine hydroxylase (TH) was significantly decreased compared to that in normal mice (Fig. 1a), indicating the loss of dopaminergic neurons in the SNpc. A previous study surveyed ACSL4 expression in the brain, and found that it was highly colocalized with neurons, but also colocalized with microglia in the cerebral cortex [30]. We further immunolabeled the brain slides with an anti-ACSL4 and anti-TH antibodies, and found that the average fluorescence intensity of ACSL4 in the SN was increased in the MPTP group, and there was colocalization of ACSL4 and TH (Fig. 1b). These results collectively indicate that ACSL4 is upregulated in the SN of parkinsonism mice.

Reduction of ACSL4 Locally in the SN Does Not Affect the Motor Functions

Upregulation of ACSL4 observed in PD may be pathological, and lowing its expression may provide therapeutical benefits. Considering that ACSL4 is a critical enzyme related to lipid peroxide accumulation [20], its reduction in SN may lead to fluctuation of lipid peroxide levels and generate side effects. To rule this concern out, we have therefore selectively knocked out ACSL4 in the unilateral SN by a single injection of adeno-associated viral vectors, namely, AAV8-EF-Cas9 and AAV8-mACSL4-sp.g3 mixed 1:1 before use (ACSL4-KO). An AAV8 with an enhanced green fluorescent protein, AAV8-EGFP, was used as a control (the EGFP group). The mice were raised for 4 weeks post-AAV injection to guarantee virus expression [31] (Fig. 1c).

The location and transduction effectiveness of AAV were investigated. Images from immunofluorescence staining indicate that EGFP-positive cells were distributed in the SN region which colocalized with TH-positive dopaminergic neurons (Fig. 1d). The percentage of EGFP-positive cells ipsilateral to the AAV injection site was 53.38 ± 4.38, while that contralateral was 2.77 ± 0.77, as detected with flow cytometry (Fig. 1e). The expression of ACSL4 ipsilateral to the AAV injection site was significantly reduced compared to that contralateral side (Fig. 1f), and the protein levels of ACSL4 were decreased in the ACSL4-KO group consistently (Fig. 1g). These results suggest that stereotaxic injection of AAV into the SN region lowered ACSL4 expression.

We then tested whether lowered ACSL4 affects the motor functions of the mice 7 weeks post-AAV injection, and found no differences in behavioral performances, evidenced by similar time to turn in the pole test between ACSL4-KO mice and EGFP mice (Fig. 1h), and unaltered stride length (Fig. 1i) in the DigiGait analysis. TH expression was also unaffected by ACSL4 reduction (Fig. 1j). Thus, lowered ACSL4 in the SN did not cause motor changes or loss of dopaminergic neurons.

ACSL4 Reduction Mitigates MPTP-Induced Motor Deficits and Dopaminergic Neuronal Loss

Since the reduction of ACSL4 in the SN was tolerable, we next investigated if such reduction may be beneficial in the MPTP PD model. The ACSL4-KO mice and EGFP mice were assigned randomly to MPTP or saline group 4 weeks post-AAV injection, and then detected the motor functions and dopaminergic neuron survival at 7 weeks (Fig. 2a). We found that the time to turn of pole test in MPTP-treated EGFP mice was significantly longer than that in saline-treated EGFP mice, an indication of motor dysfunction, while MPTP-treated ACSL4-KO mice exhibited a similar response to saline-treated EGFP mice (Fig. 2b). Consistently, compared with saline-treated EGFP control mice, the MPTP-treated EGFP mice exhibited a significantly lower stride length of the right forelimb in DigiGait analysis, whereas the MPTP-treated ACSL4-KO mice prevented the stride length changes (Fig. 2c, d). These results support that ACSL4 KO prevented the motor dysfunction induced by MPTP intoxication.

We then evaluated the TH protein expression and counted the number of TH-positive neurons in the SN stereologically. Western blot results indicated that ACSL4-KO prevented MPTP-induced reduction of TH expression (Fig. 2e). TH-positive neuron number within the left SNpc was estimated using a stereological fractionator design [9], and it was 7258 ± 602 in saline-treated EGFP mice but 5471 ± 697 in MPTP-treated EGFP mice; however, the neuron number recovered to 7018 ± 1027 in MPTP-treated ACSL4-KO mice (Fig. 2f). These results collectively suggested that ACSL4 KO protected dopaminergic neurons against MPTP neurotoxicity.

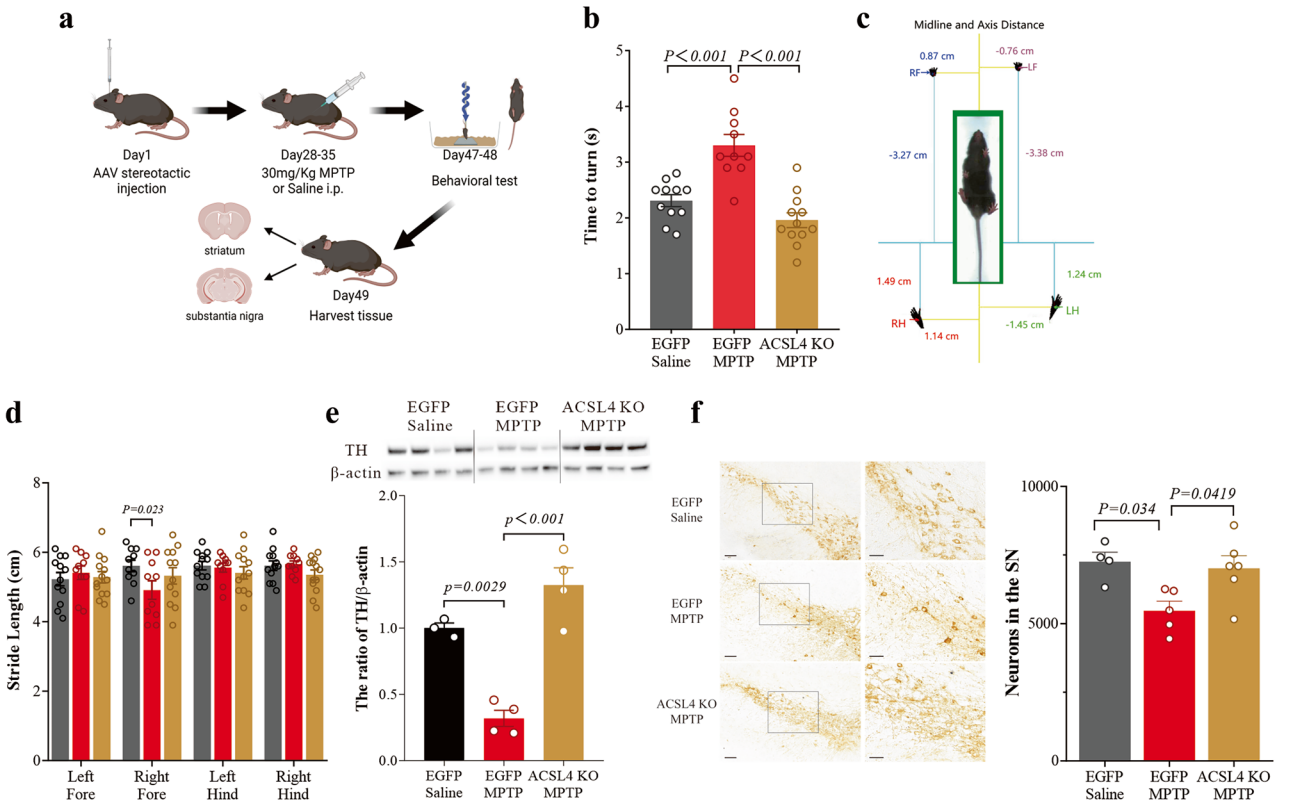

Fig. 2 Reducing ACSL4 expression ameliorates parkinsonism deficits. **a** Experimental scheme of AAV injection, model establishment, and phenotype detection. **b** Time to turn of pole test in the EGFP-saline, EGFP-MPTP, and ACSL4-KO-MPTP groups of mice. **c** Examples of footprints and the midline and axis distance were measured by the DigiGait™ analysis system and merged with a real picture of a mouse captured by the camera in the DigiGait apparatus. **d** The stride length was obtained from mice in the EGFP-saline, EGFP-MPTP, and ACSL4-KO-MPTP groups. The value on the Y-axis represents the raw data exported from the DigiGait™ analysis system. **e** The levels of TH expression in all three groups. The data are presented as the ratio of TH expression to β-actin expression and were normalized to the values in EGFP-saline mice. **f** Left, representative images of TH-positive neurons in the SN and magnified images of the ROI in each group. The scale bars represent 400 μm and 50 μm, respectively. Right, stereotactic counting of TH-positive dopaminergic neurons in the SN. Each point in the histogram represents a mouse. One-way ANOVA or two-way ANOVA followed by Tukey's post hoc multiple comparison tests were performed. The *p* values are labeled in the histogram

Triacsin C Pretreatment Ameliorates MPTP-Induced Motor Deficits and Dopaminergic Neuronal Loss

Triacsin C (1-hydroxy-3-(E,E,E-2′,4′,7′-undecatrienylidine) triazene) was identified as a strong inhibitor of ACSL1 and ACSL4 activities [29], and it can protect against ischemic brain injury through inhibition of ACSL4 activity [21]. Here, we assessed if Triacsin C protects against MPTP neurotoxicity. Indeed, there was a significant reduction in the time-to-turn in the pole test with Triacsin C pretreatment (Fig. 3a), and a significantly higher stride length of the right forelimbs (Fig. 3b, c), compared between the solvent-pretreated MPTP group and the Triacsin C-pretreated MPTP group.

Further, we have found that the MPTP-induced reduction in TH expression was also reversed following Triacsin C pretreatment (Fig. 3d). The solvent-pretreated MPTP group mice presented a significant reduction in dopamine (DA) in the striatum, where Triacsin C pretreatment ameliorated such reduction (Fig. 3e). Its metabolites dihydroxy-phenyl acetic acid (DOPAC) and homovanillic acid (HVA) levels were not different among the three groups (Fig. 3e).

Considering that Triacsin C can be a strong inhibitor for both ACSL1 and ACSL4 activities, we additionally knocked down ACSL1 in N27 rat dopaminergic neural cells and mouse neuroblastoma (N2a) cells (Fig. S1a, d), and treated with increasing doses of MPP^+. ACSL1 reduction could not prevent MPP^+-induced cell death in both

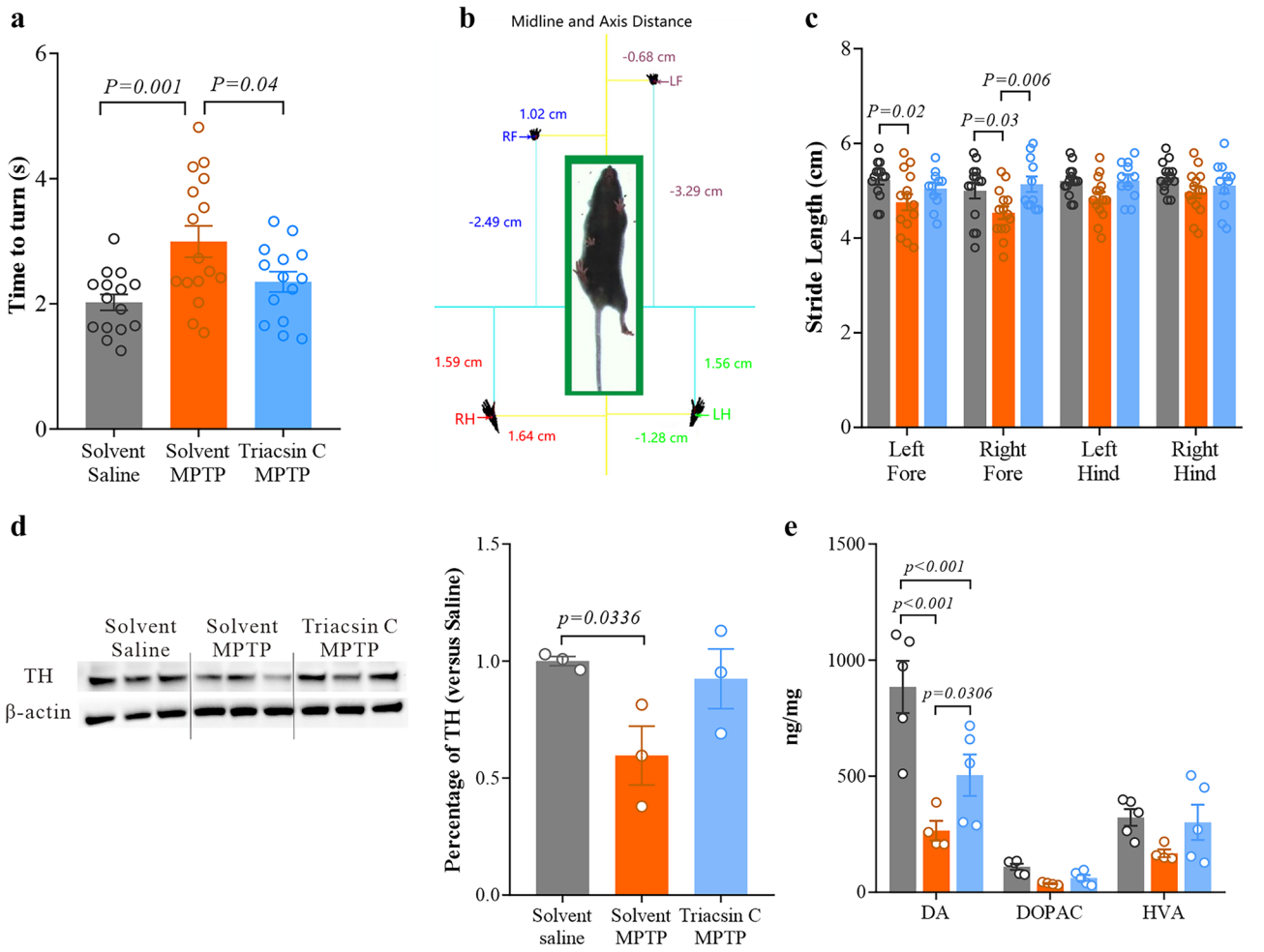

Fig. 3 Triacsin C pretreatment ameliorated parkinsonism deficits. **a** The time to turn of pole test in the solvent-saline, solvent-MPTP, and Triacsin C-MPTP groups of mice. **b** Examples of footprints and the midline and axis distance were measured by the DigiGait™ analysis system and merged with a real picture of a mouse captured by the camera in the DigiGait apparatus. **c** The stride length of DigiGait analysis for all three groups. The value on the Y-axis represents the raw data exported from the DigiGait™ analysis system. **d** The levels of TH expression in all three groups. The data were presented as the ratio of TH expression to β-actin expression and were normalized to the values in the solvent-saline mice. **e** Concentrations of DA, DOPAC, and HVA in the striatum were detected with LCMS/MS. Each point in the histogram represents a sample. One-way ANOVA or two-way ANOVA followed by Tukey's post hoc multiple comparison tests were performed. The *p* values lower than 0.05 are labeled in the histogram; otherwise, the *p* values are not displayed

cell lines (Fig. S1b, e), which is different from ACSL4 reduction. Further, we tested the contents of arachidonic acid (AA), which esterification was catalyzed by ACSL4, in N27 and N2a cells treated with Triacsin C, and found that the AA contents in both cells were increased (Fig. S1c, f), indicating that the activity of ACSL4 was reduced with Triacsin C treatment. These results support that Triacsin C alleviates the MPP^+ toxicity mainly through inhibiting ACSL4, similar to the protection observed with ACSL4 reduction.

ACSL4 Affects Lipid ROS in Models of PD

One key characteristic of ferroptosis is the accumulation of lipid ROS, and ACSL4 was previously suggested to facilitate such accumulation by promoting the esterification of AA and adrenaline into phytosterol esters [20]. Therefore, using both N27 and N2a cells with MPP^+ treatment, we have investigated the changes of intracellular ROS with modulations of ACSL4 through a ROS assay kit. We have first confirmed that ACSL4 knockdown (KD, Figs. 4a and S2a) or inhibition of its activity

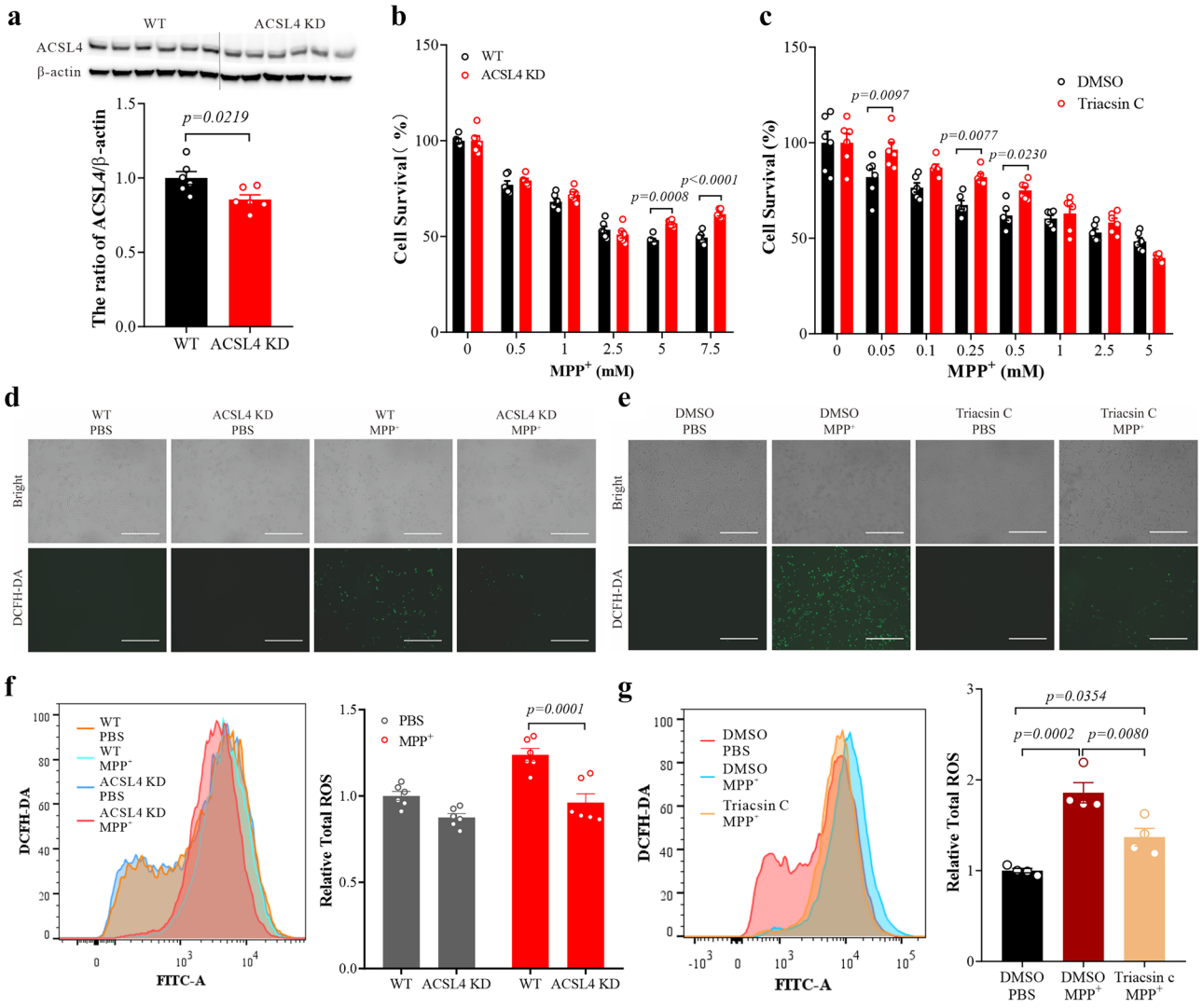

Fig. 4 Knockdown or inhibition of ACSL4 ameliorated cell death and total ROS production induced by MPP^+. **a** ACSL4 expressions in ACSL4-KD-N27 and WT-N27 cells. **b** Cell survival was discrepant between WT-N27 and ACSL4-KD-N27 cells when treated with increasing doses of MPP^+. **c** Cellular survival was different between Triacsin C-pretreated and DMSO solvent-pretreated N27 cells under treatment with increasing doses of MPP^+. **d–e** Representative bright-field white-light (top) and DCF fluorescence (bottom) schematics, showing DCFH-DA-labeled intracellular ROS in ACSL4-KD or Triacsin C-pretreated N27 cells after MPP^+ treatment. Scale bar: 200 μm. **f–g** Intracellular ROS production labeled with DCFH-DA in ACSL4-KD or Triacsin C-pretreated N27 cells was detected by flow cytometry after MPP^+ incubation. Representative histogram plot for DCF fluorescence (left) and quantification results (right). Each point in the histogram represents a sample. One-way ANOVA or two-way ANOVA followed by Tukey's post hoc multiple comparison tests or *t*-tests were performed. The *p* values lower than 0.05 are labeled in the histogram; otherwise, the *p* values are not displayed

(with Triacsin C) can promote cell survival even with increasing doses of MPP^+ (Figs. 4b, c and S2b, c), consistent with our observations in MPTP intoxicated mice. The total ROS level after MPP^+ treatment in WT cells was significantly higher than that in ACSL4-KD cells (Figs. 4d, f and S2d, f), and similar results were obtained for Triacsin C-pretreated cells (Figs. 4e, g and S2e, g), indicating that total ROS was affected by ACSL4 modulation when challenged by MPP^+ treatment.

To identify the specific sources of ROS affected by ACSL4 and MPP^+, we then assayed lipid peroxides in various experimental conditions. We detected the lipid peroxides of WT and ACSL4-KD N27 and N2a cells treated with 5 mM MPP^+ or PBS for 12 h with BODIPY 581/591 C11 through flow cytometry. The lipid ROS levels in the ACSL4-KD cells were significantly lower than those in the WT cells with MPP^+ treatment, indicating that the knockdown of ACSL4 partially prevented the increase in lipid ROS levels induced by MPP^+ (Figs. 5a and S3a). Similarly, pretreatment with Triacsin C for 48 h also partially prevented the MPP^+-induced lipid ROS elevation (Figs. 5b and S3b).

MPP^+ damages cellular mitochondria by inhibiting respiration at complex I of the electron transport chain and promotes the generation of ROS, which then contributes to an increase in intracellular oxidative stress [32]. Thus, we also detected the content of mitochondrial ROS (mitoROS) with a MitoSOX™ Red in ACSL4-KD or Triacsin C-pretreated N27 and N2a cells after MPP^+ treatment. We found that neither the knockdown of ACSL4 nor Triacsin C pretreatment prevents the MPP^+-induced mitoROS elevation (Figs. 5c, d and S3c, d), indicating that while the mitoROS is participating in MPP^+-induced neurotoxicity, the protective effects of ACSL4 is not related with mitoROS.

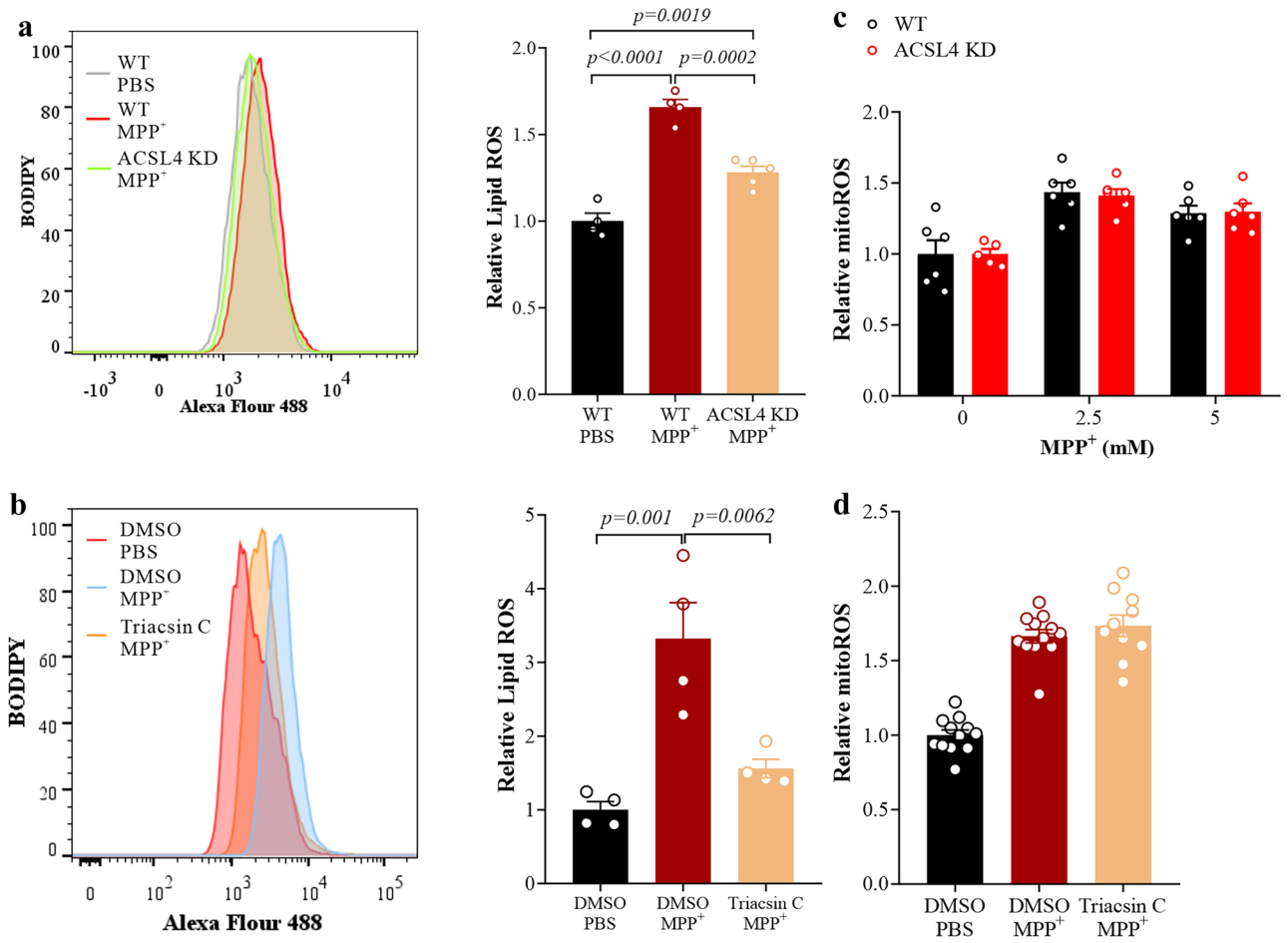

Fig. 5 Knockout or inhibition of ACSL4 ameliorated lipid ROS but not mitochondrial ROS production induced by MPP^+. Lipid ROS levels in ACSL4 KD (**a**) or Triacsin C-pretreated (**b**) N27 cells after MPP^+ treatment. Representative histogram plot for the fluorescence of oxidized BODIPY 581/591 C11 (left) and the results of quantification analysis expressed as the ratio of oxidized to reduced BODIPY 581/591 C11 mean fluorescence intensity (right). Quantification results of mitochondrial ROS detected with fluorescence microplate reader in ACSL4 KD (**c**) or Triacsin C-pretreated (**d**) N27 cells after MPP^+ treatment. Each point in the histogram represents a sample. One-way ANOVA or two-way ANOVA followed by Tukey's post hoc multiple comparison tests were performed. The p values lower than 0.05 are labeled in the histogram; otherwise, the p values are not displayed

ACSL4 Is Upregulated in Human SN of PD

A previous study has surveyed genome-wide transcriptome changes for SN pars compacta (SNpc) tissues obtained from controls and PD patients (GSE178265, the Gene Expression Omnibus, GEO, https://www.ncbi.nlm.nih.gov/gds) [33]. We wondered if the *ACSL4* expression was changed in the SNpc of PD patients, as we observed in the MPTP mice. We found that the *ACSL4* expression in dopaminergic and nondopaminergic neurons, microglia, and endothelial cells of PD patients was significantly increased (Fig. 6), consistent with our previous findings that the ACSL4 levels were elevated in SN with partial colocalization with dopaminergic neurons in the MPTP mice. These findings support the critical role of ACSL4 in PD pathogenesis.

Discussion

In the present study, we identified a crucial role of ACSL4 in PD pathogenesis. The SN ACSL4 expression was increased in PD patients and MPTP-intoxicated mice. Inhibition of ACSL4 genetically or pharmacologically attenuated MPTP-induced parkinsonism, including the motor dysfunction and TH-positive neuron reduction in the SNs of mice, as well as the MPP^+-induced cell death, collectively provides further evidence supporting that ferroptosis may be targeted for PD therapy.

Ferroptosis is triggered by the peroxidation of PUFAs and was noted in the pathogenesis of a range of diseases including several neurodegenerative diseases [5, 34, 35]. Long-chain fatty acid CoA ligases (ACSLs), which are expressed on the endoplasmic reticulum and mitochondrial outer membrane, catalyze the formation of acyl-CoAs from fatty acids and facilitate fatty acid metabolism and membrane modifications [36]. Five isoforms of ACSL (ACSL1, ACSL3, ACSL4, ACSL5, and ACSL6) have been identified in humans and rodents with similar functions, but only ACSL4 correlates with erastin-induced ferroptosis sensitivity [37]. ACSL4 was found to be affected during the progression of several diseases [21, 22], and here we found that ACSL4 potentially contributes to neuronal ferroptosis that occurred in PD.

Many key components of the ferroptotic pathway are involved in the pathology of PD, and the involvement of ferroptosis in the pathogenesis of PD has been demonstrated by in vivo and in vitro PD models [16, 17]. In PD patients, the level of iron is significantly increased in the substantia nigra of the brain, and the level of iron is closely associated with disease severity [9, 38, 39]. Targeting iron in the SN can prevent further decline in PD patients when treated with deferiprone [14]. On the other hand, due to the limited abilities of ferroptosis inhibitors to cross the blood–brain barrier, there have not been trials of PD directly targeting ferroptosis. In our present study, we directly regulated the key enzyme ACSL4 related to lipid metabolism in ferroptosis with Triacsin C, which significantly alleviated motor dysfunction and dopaminergic neuron death. Therefore, ACSL4 inhibitors may be promising for the treatment of PD.

The levels of PUFAs and lipid peroxides serve as indicators of ferroptosis. In Parkinsonian postmortem brains, the PUFA levels in the SN were lower in PD brains than in control brains, whereas the levels of the lipid peroxidation intermediate malondialdehyde were significantly higher [40]. These findings indicate that the basal lipid peroxidation in the SN is increased in PD, which may trigger ferroptosis. Another study used deuterated PUFAs (D-PUFAs) instead of essential PUFAs in mouse diets to reduce the oxidation

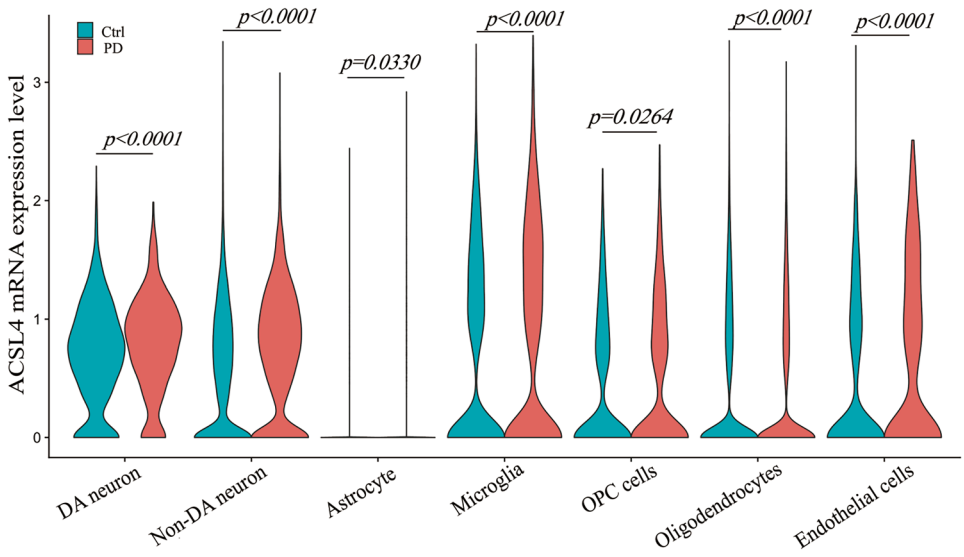

Fig. 6 ACSL4 is upregulated in human SNpc of PD. Violin plot of *ACSL4* levels in different types of cells in the SNs of PD patients using data from GSE178265, which was reanalyzed with Seurat 4.0.5, package in R, version 4.1 (R Foundation)

of PUFAs and discovered that D-PUFAs partially alleviated nigrostriatal damage from oxidative injury caused by MPTP exposure [41]. Consistent with these reports, we found here that the levels of lipid peroxides were also promoted by MPP^+ treatment, and inhibitions of ACSL4 genetically or pharmacologically lowered its level, similar to our previous findings in neuronal ischemia–reperfusion models [21].

Mitochondria play dual roles as sources and targets of ROS. Previous studies indicate that mitochondrial dysregulation and increased oxidative stress play important roles in the pathogenesis of PD. Mutation in the mitochondrial ROS scavenging-related gene *DJ-1* caused an autosomal recessive form of PD [42–44]. MPP^+/MPTP insert toxicity through disruption of ATP production in mitochondria [32, 45]. The MitoSOX™ Red we used in the current study mainly detects mitochondrial superoxide, while DCFH-DA mainly marks hydrogen peroxide and hydroxyl radicals [46]. In our results, inhibition of ACSL4 alleviated the MPP^+-induced elevation in hydrogen peroxide and hydroxyl radical levels but not the mitochondrial superoxide levels (Figs. 4f, g, 5c, d and S2f, g, 3c, d). We speculate that ACSL4 may not be involved in the production of mitochondrial superoxide at the initial stage of MPP^+ toxicity but may participate in the subsequent generation of hydrogen peroxide and hydroxyl radicals.

To summarize, we have found that ACSL4 inhibition attenuated parkinsonism phenotypes in mice, and the protective effect may be specifically associated with the prevention of lipid ROS elevation. These data support ACSL4 as a therapeutic target associated with lipid peroxidation in PD.

Materials and Methods

Animals

Wild-type (C57Bl/6) (WT) mice were purchased from Chongqing Ensiweier Biotechnology Co. Ltd. and housed and bred at a density of at most five animals per cage with water and food ad libitum under a 12 h light/dark cycle. Mice aged 3–4 months were selected and randomly assigned (by Microsoft Excel) to either the control group or the treatment group. All animal studies were performed following the experimental guidelines of the Institutional Guidelines of the Animal Care and Use Committee (K2018071) of Sichuan University.

To induce parkinsonism in mice, 30 mg/kg MPTP (M0896, Sigma) was intraperitoneally injected once a day for 8 days. For the control mice, only saline was injected. For Triacsin C treatment, 25 μL of 0.5 mg/mL Triacsin C (10,007,448, Cayman Chemical) or an equal volume of vehicle (10% DMSO, 5% Tween-80, 10% PEG 400, 75% saline) was administered intranasally 2 h before MPTP or saline injection.

sgRNA Design and Adeno-Associated Viral Vector Production

sgRNA design and adeno-associated viral vector were produced as previously described [21]. Briefly, online tools (http://crispr.mit.edu/, https://crispr.cos.uniheidelberg.de/, and http://asia.ensembl.org/) were used to determine the sgRNAs and their target sequences for gene editing. The sgRNAs were then separately inserted into BbsI-cleaved pssAAV-EF-gRNA to generate sgRNA-containing plasmids and Cas9 expression plasmids. Two kinds of plasmids and a plasmid for control EGFP expression were used to produce the rAAV vector in serotype 8 (rAAV8); the resulting constructs were named ssAAV8-mACSL4-sp.g3, ssAAV8-EF-cas9, and ssAAV8-CB-EGFP. All of the AAV8 vectors were generated, collected, purified, and titrated as described previously [47], and then aliquoted and stored at − 80 °C until use.

Stereotaxic Injection

AAV8 micro-injections were performed 4 weeks before MPTP injection. Mice were anesthetized with a cocktail of 10 mL/kg 2% chloral hydrate and 8% urethane (BBI Life Science) and then placed on a stereotaxic apparatus (68,037, RWD). After sterilizing the head and drilling the skull, a glass electrode filled with 1 μL of ssAAV8-mACSL4-sp.g3 (1×10^{13} GC/mL) and 1 μL of ssAAV8-EF-cas9 (1×10^{13} GC/mL) or 2 μL of ssAAV8-CB-EGFP (1×10^{13} GC/mL) aimed at the left SN (AP: − 3.1 mm, ML: − 1.2 mm, DV: − 4 mm from the dura) was used for injection. rAAV2/9-hSyn-EGFP-WPRE-pA was used for injection to identify whether the injection site was in the SN during the preliminary experiment. The animals were randomly assigned to the ACSL4-KO group or the EGFP control group as described previously. The injection was conducted at a rate of 100 nL per min, and then the glass electrode was left in place for another 5 min after injection before being withdrawn slowly. The scalp was sutured, and proper postoperative care was given until the mouse awakened. At 29 days post-injection, the mice have been randomly selected for MPTP or saline intoxication.

Motor Functional Test

For the pole test, mice were placed vertically (head-up) on a 50 cm vertical, 1 cm diameter pole. On the day prior to testing, the animals were habituated to the pole and were subjected to five consecutive trials. Then, on the second day, the animals were recorded via digital video to cover the whole process of climbing down. The duration was recorded for the mouse to turn toward the ground (time to turn). Trials with events such as slipping off or falling to

the ground were excluded. Five intact trials were counted for each mouse, and the average time was used for analysis.

For the gait analysis, a DigiGait™ imaging system (Mouse Specific, Inc.) was used to record and analyze the movement status of the mice. Specifically, each mouse was placed on a transparent mechanical belt. The speed of the belt was 15 cm/s, which was determined according to the principle that the mouse should be able to walk steadily at that speed; if at a lower speed, the mouse would walk in an exploratory manner, while at a higher speed, the mouse would be unable to walk. A high-speed camera captured video of the mouse walking, and then a section in which the mouse walked stably for approximately 4 s was selected for analysis using the DigiGait™ analysis 15 system (Mouse Specifics, Inc.).

Western Blot Analysis

Mice were deeply anesthetized and perfused with ice-cold PBS (0.01 M) transcardially. The brain was removed, and the striatum and SN were immediately dissected on ice. The SN was homogenized with RIPA lysis buffer composed of 50 mM Tris–HCl (pH = 7.6), 150 mM NaCl, 1% (v/v) Triton X-100, protease inhibitor cocktail (1:50, Roche), and phosphatase inhibitors II and III (1:1000) on ice for 30 min. After centrifugation at 13,000 × g for 20 min at 4 °C, the supernatants were harvested for analysis. The protein concentration was calculated with a BCA protein assay kit (Beyotime). An equal amount of protein from each sample was mixed with loading buffer, denatured at 100 °C for 5 min, and then separated by 4–20% SDS polyacrylamide gels, and the protein in the gel was transferred to a PVDF membrane (Millipore). After blocking in 5% nonfat milk for 1 h at room temperature, the membranes were incubated overnight at 4 °C with primary antibodies and then incubated for 2 h at room temperature with a secondary IgG-HRP conjugated antibody (1:10,000, Santa Cruz Biotechnology). An enhanced chemiluminescence detection system (Thermo Scientific) was used for development, Bio-Rad's ChemiDoc XRS + system was used for visualization, and ImageJ (1.49 m, NIH) software was used to quantify the immunoreactive signals. The antibodies used for this study targeted TH (1:5000, Merck, ab152), ACSL4 (1:1000, Abcam, ab155282), ACSL1 (1:1000, cell signaling technology, 9189), and β-actin (1:5000, Abcam, ab179467).

Immunofluorescence and Immunohistochemical Analyses

Mice were perfused with ice-cold 0.01 M PBS followed by 4% paraformaldehyde (PFA) in PBS transcardially. Then, the brain was removed and postfixed in 4% PFA overnight. After cryoprotection in 30% sucrose at 4 °C for 2–3 days, the SN was cut into 30 μm sections on a cryostat microtome (CM1860, Leica). The sections were blocked in 6% normal goat serum (Solarbio, SL038) for 2 h at room temperature and then incubated with a primary antibody against TH (1:1000, Merck, ab152) overnight at 4 °C.

For immunohistochemistry, the sections were incubated with a secondary HRP-conjugated goat anti-rabbit antibody for 3 h at room temperature followed by diaminobenzidine solution (1:50, Abcam, ab64238) for 12 s and then covered with coverslips. After that, the number of neurons within the SNpc was estimated using a stereological fractionator design.

For immunofluorescence, the sections were then incubated with a CY3-conjugated goat anti-rabbit secondary antibody (1:1000, Abcam, ab6953) for 3 h at room temperature in the dark and mounted on Superfrost-Plus slides with 4,6-diamidino-2-phenylindole (DAPI) in 80% glycerin to stain the nuclei. The labeled sections were imaged with a confocal microscope (Zeiss, LSM 880).

Stereological Estimation of Nigral Dopaminergic Neuron Number

The TH-positive neurons in the SNpc (left and right hemispheres, respectively) were estimated using an automated physical detector in the splitter design of the virtual slide as previously described [9]. Briefly, sampling was carried out on a Leica DM4 B Digital microscope hard-coupled to a MAC 6000 controller module, and implemented using the Stereo Investigator software package (MicroBrightField Inc.). After delineating the SNpc at low magnification (10 × objective, N.A. 0.25), a sampling grid was overlaid on the tracking area and individual immune-stained cell bodies were visualized using a 40 × objective (N.A. 0.8). Only the cells with a visible nucleus that were clearly TH-immunopositive were counted with the following parameters: the counting frame was 45 μm × 45 μm (height × width), the sampling grid was 140 μm × 140 μm. The experimenter was blinded to all experimental conditions. The coefficient of error (CE) Gunderson ($m = 1$) values were < 0.1 for all animals.

Dopamine and DOPAC Measurements

The striatum dissected from the mouse brain was homogenized with water (Optima™ LC/MS Grade, Fisher Chemical) and then sufficiently mixed with acetonitrile (Optima™ LC/MS Grade, Fisher Chemical). After that, the samples were centrifuged at 12,000 rpm for 10 min at 4 °C, and the supernatants were harvested, filtered, and evaporated sequentially. Before detecting DA and its metabolites

DOPAC and HVA in all samples in the LC–MS/MS system (AB SCIEX QTRAP 5500), the samples were redissolved in acetonitrile and then injected onto a chromatographic column (ACQUITY UPLIC HSS T3 1.8 m). The measurement conditions during analyses were as follows: column temperature 40 °C, mobile phase A: 0.1% acetic acid in water (acetic acid:water = 1:1000, v/v), mobile phase B: 0.1% acetic acid in acetonitrile (acetic acid:acetonitrile = 1:1000, v/v), flow rate 0.4 mL/min; gradient: A 90% 0–1 min, 10% 1–2.5 min, and equilibration time of 2.5 min. Mass spectrometry analysis was performed in negative electrospray ionization mode.

Cell Culture and Viability Assays

N27 cells (Merck, Bayswater, Australia) were cultured in RPMI 1640 (Gibco, Thermo Fisher Scientific) supplemented with 10% fetal bovine serum (Gibco, Thermo Fisher Scientific) and 1% penicillin–streptomycin in a humid incubator at 37 °C with 5% CO_2. N2a cells (National Collection of Authenticated Cell Cultures) were cultured in DMEM (Gibco, Thermo Fisher Scientific) supplemented with 10% fetal bovine serum (Gibco, Thermo Fisher Scientific) and 1% penicillin–streptomycin in a humid incubator at 37 °C with 5% CO_2. Cells were seeded onto 96-well plates and then treated with Triacsin C, DMSO, or MPP^+ (Sigma, D048) after plating. Specifically, N27 or N2a cells were pretreated with 3 or 10 μM Triacsin C or 0.0125% DMSO for 48 h and then treated with 0.5–5 mM MPP^+ for 24 h. The ACSL4-KD or WT N27 and N2a cells were treated with 0.5–7.5 mM MPP^+. The ACSL1-KD or WT N27 and N2a cells were treated with 0.1–7.5 mM MPP^+. Then, cell viability was assessed using an MTT cytotoxicity assay kit (Sigma, M2003) as previously described [9].

Establishment of ACSL1 and ACSL4-Knockdown Cells

Guide RNA (gRNA) was designed to specifically cut the first exon of the ACSL4 gene and the first exon of the ACSL1 gene in the mouse genome (*ACSL4*: Ensembl sequence ENSMUSG00000031278; *ACSL1*: Ensembl sequence ENSMUSG00000018796) and rat genome (*ACSL4*: Ensembl sequence ENSRNOG00000019180; *ACSL1*: Ensembl sequence ENSRNOG00000010633). The ACSL4- or ACSL1-guided RNA sequence was cloned into a lentiCRISPRv2 vector, and the resulting construct was named sgACSL4-lentiCRISPRv2 or sgACSL1-lentiCRISPRv2. The N2a and N27 cells were then transfected with either sgACSL4-lentiCRISPRv2 or scramble DNA using Lipofectamine 3000 (Invitrogen Waltham, MA) according to the manufacturer's instructions to obtain ACSL4-KD or WT cells, and also transfected with either sgACSL1-lentiCRISPRv2 or scramble DNA to obtain ACSL1-KD or WT cells. Specifically, N2a or N27 cells were seeded in 6-well plates and maintained in DMEM or RPMI 1640 supplemented with 10% FBS and 1% penicillin/streptomycin. When the cells reached 70% confluence, 250 μL of Opti-MEM containing 2.5 μg of plasmid sgACSL4-lentiCRISPRv2 or sgACSL1-lentiCRISPRv2 or scramble DNA, 5 μL of P3000 reagent, and 3.75 μL of Lipofectamine 3000 reagent were added, and the cells were incubated for 6 h. The medium was then replaced with DMEM or RPMI 1640 (containing 10% FBS and 1% penicillin/streptomycin). After 48 h, the cells were harvested and analyzed for ACSL4 or ACSL1 expression by western blotting.

Assessment of ROS

N27 cells were pretreated with 10 μM Triacsin C or 0.0125% DMSO for 48 h and then treated with 5 mM MPP^+ for 12 h. Meanwhile, N2a cells were pretreated with 3 μM Triacsin C or 0.0125% DMSO for 48 h and then treated with 3 mM MPP^+ for 12 h. The ACSL4-KD or WT N27 cells were treated with 5 mM MPP^+ for 12 h, while ACSL4-KD or WT N2a cells were treated with 3 mM MPP^+ for 12 h. Then, the cells were collected and washed with DPBS (Gibco).

For BODIPY staining, the collected cells were incubated in 1 mL of HBSS with 5 μM BODIPY 581/591 C11 (Thermo Fisher) for 20 min at 37 °C. Using the 488 nm laser of a flow cytometer (LSR Fortessa, BD) for excitation, the signals from both oxidized C11 (FITC channel) and non-oxidized C11 (PE channel) were monitored. The ratio of the mean fluorescence intensity (MFI) of FITC to the MFI of PE was calculated as the relative lipid ROS for each sample by using FlowJo software (version 10).

To determine the intracellular ROS, a reactive oxygen species assay kit (S0033, Beyotime, Nanjing, China) with the fluorescent probe 2′,7′-dichlorofluorescein-diacetate (DCFH-DA) was used. The collected cells were incubated with the fluorescent probe for 20 min. Subsequently, the dichlorofluorescein (DCF) fluorescence intensity was detected in the FITC channel. In addition, the cells cultured in 6-well plates were incubated with the kit reagent immediately, and then the fluorescence intensity was detected with fluorescence microscopy (Olympus).

MitoSOX™ Red superoxide indicator (M36008, Thermo Fisher) was used to assess mitochondrial ROS production. For N2a cells, the collected cells were incubated with 5 μM MitoSOX Red for 20 min at 37 °C. Then, the signal obtained from the BV510 channel was monitored following the manufacturer's guidelines. For N27 cells, the cells in plates were also incubated with 5 μM MitoSOX Red for 20 min at 37 °C, and the signal obtained at excitation/emission = 510/580 nm by using a fluorescence microplate reader (BioTek Instruments, Inc.).

Detection of Arachidonic Acid in Triacsin C-Treated Cells

Mouse or rat arachidonic acid (AA) ELISA kit (LE-M2345 or LE-B1294, LaiEr Bio-Tech, China) was used to detect the free AA level in lysates of cells following the manufacturer's protocols. N27 or N2a cells were pretreated with 10 μM Triacsin C or 0.0125% DMSO for 48 h, and then the cells were collected and washed with DPBS (Gibco). The freeze–thaw process was repeated several times until the cells were fully lysed. The lysates were centrifuged for 10 min at 3000 rpm at 2–8 °C, and the supernatants were collected to carry out the assay. In each microtiter well pre-coated with anti-AA antibody, 50 μL standard or sample was added, and then 100 μL of HRP-conjugate reagent was added to each well, covered with an adhesive strip and incubated for 60 min at 37 °C. Each well was aspirated and washed for five washes. The chromogen solution A (50 μL) and B (50 μL) were added to each well, and the solution was gently mixed and incubated for 15 min at 37 °C. Fifty microliters of Stop Solution was then added, and the optical density (O.D.) at 450 nm was recorded using a microtiter plate reader within 15 min.

Statistical Analysis

The data from the human single-cell transcriptome database GSE178265 was reanalyzed with Seurat 4.0.5, package in R, version 4.1 (R Foundation) to examine the *ACSL4* level with a Wilcoxon test.

The experimental results were analyzed with GraphPad Prism 7.0 statistical software, and the data are expressed as the mean ± SEM. An unpaired *t*-test was used to compare two groups, and one-way analysis of variance (ANOVA) or two-way ANOVA followed by Tukey's post hoc multiple comparison test was used to compare multiple groups. $p < 0.05$ was considered statistical significance.

Supplementary Information The online version contains supplementary material available at https://doi.org/10.1007/s13311-023-01382-4.

Required Author Forms Disclosure forms provided by the authors are available with the online version of this article.

Author Contribution P. Lei conceived, raised funds for, and supervised the overall project. H. X. raised funds and supervised the project. F. T., H. X., Y.-j G., and L.-l J. carried out the animal experiments. F. T., L.-y Z., and K. C. performed cell culture experiments. X.-l D. analyzed the human single-cell transcriptome data. S.-y H. performed dopamine and DOPAC measurements. P. Li and B. D. performed AAV-related experiments. F. T., H. X., R.-x X., and P. Lei integrated the data and wrote the drafts of the manuscript. All authors edited the manuscript.

Funding This work was supported by the National Natural Science Foundation of China (31800899), the Sichuan Science and Technology Program (2019YFS0212), the National Clinical Research Center for Geriatrics of West China Hospital (Z2021LC001), and the West China Hospital 1.3.5 project for disciplines of excellence (ZYYC20009).

Data Availability All data used in this study are available from the corresponding authors upon reasonable request.

Declarations

Conflict of Interest The authors declare no competing interests.

References

1. GBD 2016 Neurology Collaborators. Global, regional, and national burden of neurological disorders, 1990–2016: a systematic analysis for the Global Burden of Disease Study 2016. Lancet Neurol. 2019;18:459–80.
2. Armstrong MJ, Okun MS. Diagnosis and treatment of Parkinson disease: a review. JAMA. 2020;323:548–60.
3. Mahoney-Sanchez L, Bouchaoui H, Ayton S, et al. Ferroptosis and its potential role in the physiopathology of Parkinson's disease. Prog Neurobiol. 2021;196:101890.
4. Venderova K, Park DS. Programmed cell death in Parkinson's disease. Cold Spring Harb Perspect Med. 2012;2.
5. Yan HF, Zou T, Tuo QZ, et al. Ferroptosis: mechanisms and links with diseases. Signal Transduct Target Ther. 2021;6:49.
6. Dixon SJ, Lemberg KM, Lamprecht MR, et al. Ferroptosis: an iron-dependent form of nonapoptotic cell death. Cell. 2012; 149:1060–72.
7. Guo J, Tuo QZ, Lei P. Iron, ferroptosis, and ischemic stroke. J Neurochem. 2023.
8. Ayton S, Lei P. Nigral iron elevation is an invariable feature of Parkinson's disease and is a sufficient cause of neurodegeneration. Biomed Res Int. 2014;2014:581256.
9. Lei P, Ayton S, Finkelstein DI, et al. Tau deficiency induces parkinsonism with dementia by impairing APP-mediated iron export. Nat Med. 2012;18:291–5.
10. Lei P, Ayton S, Appukuttan AT, et al. Clioquinol rescues parkinsonism and dementia phenotypes of the tau knockout mouse. Neurobiol Dis. 2015;81:168–75.
11. Ayton S, Lei P, Duce JA, et al. Ceruloplasmin dysfunction and therapeutic potential for Parkinson disease. Ann Neurol. 2013;73:554–9.
12. Ayton S, Lei P, Adlard PA, et al. Iron accumulation confers neurotoxicity to a vulnerable population of nigral neurons: implications for Parkinson's disease. Mol Neurodegener. 2014;9:27.
13. Kaur D, Yantiri F, Rajagopalan S, et al. Genetic or pharmacological iron chelation prevents MPTP-induced neurotoxicity in vivo: a novel therapy for Parkinson's disease. Neuron. 2003;37:899–909.
14. Devos D, Moreau C, Devedjian JC, et al. Targeting chelatable iron as a therapeutic modality in Parkinson's disease. Antioxid Redox Signal. 2014;21:195–210.
15. Grolez G, Moreau C, Sablonniere B, et al. Ceruloplasmin activity and iron chelation treatment of patients with Parkinson's disease. BMC Neurol. 2015;15:74.
16. Van Do B, Gouel F, Jonneaux A, et al. Ferroptosis, a newly characterized form of cell death in Parkinson's disease that is regulated by PKC. Neurobiol Dis. 2016;94:169–78.
17. Tian Y, Lu J, Hao X, et al. FTH1 inhibits ferroptosis through ferritinophagy in the 6-OHDA model of Parkinson's disease. Neurotherapeutics. 2020;17:1796–812.
18. Zuo Y, Xie J, Li X, et al. Ferritinophagy-mediated ferroptosis involved in paraquat-induced neurotoxicity of dopaminergic neurons: implication for neurotoxicity in PD. Oxid Med Cell Longev. 2021;2021:9961628.
19. Bai L, Yan F, Deng R, et al. Thioredoxin-1 rescues MPP(+)/MPTP-induced ferroptosis by increasing glutathione peroxidase 4. Mol Neurobiol. 2021;58:3187–97.

20. Kagan VE, Mao G, Qu F, et al. Oxidized arachidonic and adrenic PEs navigate cells to ferroptosis. Nat Chem Biol. 2017;13:81–90.
21. Tuo QZ, Liu Y, Xiang Z, et al. Thrombin induces ACSL4-dependent ferroptosis during cerebral ischemia/reperfusion. Signal Transduct Target Ther. 2022;7:59.
22. Qu XF, Liang TY, Wu DG, et al. Acyl-CoA synthetase long chain family member 4 plays detrimental role in early brain injury after subarachnoid hemorrhage in rats by inducing ferroptosis. CNS Neurosci Ther. 2021;27:449–63.
23. Luoqian J, Yang W, Ding X, et al. Ferroptosis promotes T-cell activation-induced neurodegeneration in multiple sclerosis. Cell Mol Immunol. 2022;19:913–24.
24. Li Y, Feng D, Wang Z, et al. Ischemia-induced ACSL4 activation contributes to ferroptosis-mediated tissue injury in intestinal ischemia/reperfusion. Cell Death Differ. 2019;26:2284–99.
25. Liu Y, Zhang Z, Yang J, et al. lncRNA ZFAS1 positively facilitates endothelial ferroptosis via miR-7-5p/ACSL4 axis in diabetic retinopathy. Oxid Med Cell Longev. 2022;2022:9004738.
26. Duan J, Wang Z, Duan R, et al. Therapeutic targeting of hepatic ACSL4 ameliorates NASH in mice. Hepatology. 2022;75:140–53.
27. Brauer R, Bhaskaran K, Chaturvedi N, et al. Glitazone treatment and incidence of Parkinson's disease among people with diabetes: a retrospective cohort study. PLoS Med. 2015;12:e1001854.
28. Laloux C, Petrault M, Lecointe C, Devos D, Bordet R. Differential susceptibility to the PPAR-gamma agonist pioglitazone in 1-methyl-4-phenyl-1,2,3,6-tetrahydropyridine and 6-hydroxydopamine rodent models of Parkinson's disease. Pharmacol Res. 2012;65:514–22.
29. Kim JH, Lewin TM, Coleman RA. Expression and characterization of recombinant rat Acyl-CoA synthetases 1, 4, and 5. Selective inhibition by triacsin C and thiazolidinediones. J Biol Chem. 2001;276:24667–73.
30. Cui Y, Zhang Y, Zhao X, et al. ACSL4 exacerbates ischemic stroke by promoting ferroptosis-induced brain injury and neuroinflammation. Brain Behav Immun. 2021;93:312–21.
31. Tao R, Xiao L, Zhou L, et al. Long-term metabolic correction of phenylketonuria by AAV-delivered phenylalanine amino lyase. Mol Ther Methods Clin Dev. 2020;19:507–17.
32. Subramaniam SR, Chesselet MF. Mitochondrial dysfunction and oxidative stress in Parkinson's disease. Prog Neurobiol. 2013;106–107:17–32.
33. Kamath T, Abdulraouf A, Burris SJ, et al. Single-cell genomic profiling of human dopamine neurons identifies a population that selectively degenerates in Parkinson's disease. Nat Neurosci. 2022;25:588–95.
34. Yan HF, Tuo QZ, Yin QZ, Lei P. The pathological role of ferroptosis in ischemia/reperfusion-related injury. Zool Res. 2020;41:220–30.
35. Tuo QZ, Zhang ST, Lei P. Mechanisms of neuronal cell death in ischemic stroke and their therapeutic implications. Med Res Rev. 2022;42:259–305.
36. Grevengoed TJ, Klett EL, Coleman RA. Acyl-CoA metabolism and partitioning. Annu Rev Nutr. 2014;34:1–30.
37. Yuan H, Li X, Zhang X, Kang R, Tang D. Identification of ACSL4 as a biomarker and contributor of ferroptosis. Biochem Biophys Res Commun. 2016;478:1338–43.
38. Hirsch EC, Brandel JP, Galle P, Javoy-Agid F, Agid Y. Iron and aluminum increase in the substantia nigra of patients with Parkinson's disease: an X-ray microanalysis. J Neurochem. 1991;56:446–51.
39. Davies KM, Hare DJ, Bohic S, et al. Comparative study of metal quantification in neurological tissue using laser ablation-inductively coupled plasma-mass spectrometry imaging and X-ray fluorescence microscopy. Anal Chem. 2015;87:6639–45.
40. Dexter DT, Carter CJ, Wells FR, et al. Basal lipid peroxidation in substantia nigra is increased in Parkinson's disease. J Neurochem. 1989;52:381–9.
41. Shchepinov MS, Chou VP, Pollock E, et al. Isotopic reinforcement of essential polyunsaturated fatty acids diminishes nigrostriatal degeneration in a mouse model of Parkinson's disease. Toxicol Lett. 2011;207:97–103.
42. Andres-Mateos E, Perier C, Zhang L, et al. DJ-1 gene deletion reveals that DJ-1 is an atypical peroxiredoxin-like peroxidase. Proc Natl Acad Sci U S A. 2007;104:14807–12.
43. Perier C, Bove J, Dehay B, et al. Apoptosis-inducing factor deficiency sensitizes dopaminergic neurons to parkinsonian neurotoxins. Ann Neurol. 2010;68:184–92.
44. Huang Y, Wei J, Cooper A, Morris MJ. Parkinson's disease: from genetics to molecular dysfunction and targeted therapeutic approaches. Genes Dis. 2022.
45. Finkel T. Signal transduction by reactive oxygen species. J Cell Biol. 2011;194:7–15.
46. Baek SH, Cho Y, Lee J, et al. Intracellular and mitochondrial reactive oxygen species measurement in primary cultured neurons. Bio Protoc. 2018;8: e2871.
47. Wang Q, Dong B, Firrman J, et al. Efficient production of dual recombinant adeno-associated viral vectors for factor VIII delivery. Hum Gene Ther Methods. 2014;25:261–8.